Characterization of the Variability of the Strehl Ratio of Adaptive Optics Point Spread Functions

Julian C. Christou[ad], Szymon Gladysz[bd], Michael Redfern[b], L. William Bradford[c] & Lewis C. Roberts Jr. [c]

[a] *Division of Astronomical Sciences, National Science Foundation, Arlington, VA 22230, USA*
[b] *Department of Experimental Physics, National University of Ireland, Galway, Ireland*
[c] *The Boeing Company, Kihei, HI 96753, USA*
[d] *Center for Adaptive Optics, University of California, Santa Cruz, CA 95064, USA*

Abstract

We have investigated both the temporal variability of the closed-loop adaptive optics (AO) point spread function (PSF) from two different AO systems at the 3m Shane Telescope at Lick Observatory (LO) and at the 3.6m AEOS at Haleakala. The "instantaneous" Strehl ratios were obtained directly from the short-exposure data for the LO observations and from Fourier propagating the measured residual wavefront slopes for the AEOS data. Both data sets show similar behaviour with large variations in performance over short time scales. For both sets of data under quasi-stationary conditions, the distribution of the Strehl ratio shows a negative skewness. We have determined a probability density for the instantaneous Strehl ratio distribution and also the corresponding residual phase variance distribution.

Keywords: adaptive optics, system performance, Strehl ratio, natural guide stars

1. INTRODUCTION

Baldwin *et al*. have shown that selection of the best short-exposure speckle images without adaptive optics (AO) can significantly improve final image quality [1]. This "lucky exposures" imaging prompted our study of the closed-loop AO short-exposure images to investigate how effective this approach would be for closed-loop AO imaging given that AO systems stabilize the image quality. To do this, we have investigated instantaneous performance of two different AO systems by looking at the Strehl ratio S of short-exposure images which essentially "freeze" the atmospheric compensation.

Measurements of the instantaneous performance of two separate natural guide star adaptive optics (AO) systems were obtained. The first is the 61 actuator infrared Lick Observatory (LO) system mounted at the 3m Shane Telescope at Mt. Hamilton, CA and the second is the 941 actuator visible system mounted on the 3.6m Advanced Electro Optical System (AEOS) on Haleakala, Maui. For the LO system, we used the FastSub mode on the IRCAL camera to take K-band ($\lambda = 2.2\mu$m) short exposure images with typical exposure times of 22ms although some data had exposures of 57ms. The frame read time was ~ 30ms. The short-exposures essentially freeze the compensation, so that residual image motion due to the tip-tilt correction did not affect our analysis. In contrast, no high-speed focal plane data was available for the AEOS system. However, we used bursts of 1000-2000 pupil-plane wavefront slope measurements obtained at a frame rate of 200Hz and reconstructed the closed-loop residual phases from these slopes. These residual phase maps were then numerically propagated through the obscured ideal 3.6m aperture to generate the corresponding PSFs at the sensing wavelength of 0.625μm. Thus, only the residual atmospheric aberrations affected the PSFs neglecting static aberrations in the imaging leg of the optical system.

Strehl ratio measurements were obtained for both sets of focal plane images and these measurements have allowed us to investigate not only the temporal variability of the instantaneous Strehl ratio but also to compare its distribution to models allowing us to develop a probability density function (PDF) of the Strehl ratios and the corresponding phase variances in this mode of operation. Preliminary results from the LO data have been previously presented [2]. The AEOS data also permits us to investigate the how well the Strehl ratio can be estimated from the residual phase variance using the Marechal approximation.

2. OBSERVATIONS AND DATA ANALYSIS

We observed a number of single stars during a sequence of natural guide star (NGS) engineering nights in the latter half of 2005 with Lick Observatory AO system. Each data set comprised at least ten thousand 64 × 64 pixel images

taken in ten groups of one thousand each. A series of one thousand sky frames were obtained 20″ away from each object before and after each object observation. In the *K*-band data where the diffraction-limit is 151 mas, the data were effectively Nyquist sampled with a pixel scale of 76 mas/pixel. All observations were made close to the zenith (≤ 10°) and using the highest possible closed-loop frame rate. Each frame from the 1000 frame data set was flat-field corrected and sky-subtracted and then processed with a peak-tracking algorithm. This algorithm locates the peak in each of the images and locates its sub-pixel value by computing the centroid of a 3 × 3 pixel box centered on the peak pixel. This box is big enough to contain the diffraction-limited core of the AO PSF. Each frame is then shifted by computing its Fourier transform and applying a slope to the Fourier phases corresponding to the offset of the sub-pixel peak location from the frame center, i.e. pixel (33,33), and then computing the inverse Fourier transform. The procedure is repeated until a tolerance of 0.02 pixels (~ 2 mas) is reached. This represents Fourier interpolation and retains the Fourier structure of the data unlike other interpolation procedures such as the bi-cubic spline. Besides computing the sub-pixel peak location and the interpolated peak value, the algorithm also saves the peak-shifted version for each frame as well as the co-added raw frames, i.e. the long exposure, and the co-added shifted frames, i.e. the shift-and-add (SAA) image. For this analysis the latter 950 frames were used as the first 50 were contaminated by a variable bias due to the chip readout. For the AEOS data, typically 1000 – 2000 residual phase maps were obtained in a quick burst mode at 200Hz and these were numerically propagated through the ideal pupil generating oversampled, by close to a factor of two, PSFs. Unlike the LO observations these data were additive noise free. The same sub-pixel peak-tracking algorithm was applied but using a 5 × 5 pixel box centered on the peak pixel to locate the peak centroid.

Computing the Strehl ratio for the AEOS data was very straightforward. A phase screen of zero radians was propagated through the aperture as were the reconstructed phase screens. The peak value was found in the same way as for the measurements and each peak value was then normalized by that value. The lack of pixel binning and read noise meant that there was no scaling problem. It was more problematic for the LO data. An ideal PSF for the telescope was computed numerically at an 8× higher spatial resolution than the Nyquist-sampled data. This was done by computing an annular aperture at the corresponding pupil-plane scale using "soft" edges, i.e. by using fractional pixel intensity values when the edge of the pupil is not fully sampled by a pixel. From Fourier optics the PSF is simply the power spectrum of this annulus. The effect of pixel binning is then simulated by binning the PSF from the original 512 × 512 pixel size to the final 64 × 64 pixel size keeping the same field size. This has been found to yield significantly more accurate Strehl ratios when comparing the measured PSFs to either numerically or analytically derived ones PSFs generated with the correct sampling but without the binning effects accounted for [3].

The SAA images were found to have a small residual bias, typically less than a count, which was subtracted. This residual bias was estimated from the intensity histogram of the SAA image. The additive noise in the image showed as a Gaussian with a mean close to, but not at, zero. The ideal PSF and SAA image were then normalized to have the same power within a radius of 25 pixels (1.9 arcseconds). This aperture was determined by investigating the images to ascertain when the noise floor was reached. The ratio of the normalized SAA images to that of the normalized ideal PSF then gives the Strehl ratio (*S*) for each SAA image. The peak value of the shift-and-add image and its corresponding Strehl ratio yields a correction factor which, when applied to the peak values of the individual frames used to generate the SAA image, gives their individual Strehl ratios. Furthermore, the variance in these correction factors (σ_c^2) yields an uncertainty in the Strehl ratio determination for the shift-and-add images for a particular data set. The advantage of computing the Strehl ratio in this manner is that, by using the shift-and-add images, it is computed on a significantly higher SNR (31×) image than for an individual frame. Furthermore, the shift-and-add images ensure that the peak value is centered on a single pixel. This is not necessarily the case for the long exposures and their Strehl ratios were computed after applying the same Fourier shift.

Fig. 1 shows examples of the instantaneous variation in *S* for some of the LO measurements. The top four plots show relatively stationary performance for four different stars with a significant dispersion in the mean for each. The bottom four plots, from a different night, illustrate the performance variability on a single star observed transiting near the zenith for just over an hour's worth of measurements. Fig. 2 shows the histograms of *S* for the quasi-stationary data. All four show a similar negative skewness which is the opposite of that seen for speckle data which has a high Strehl ratio tail where the "lucky exposures" are situated.

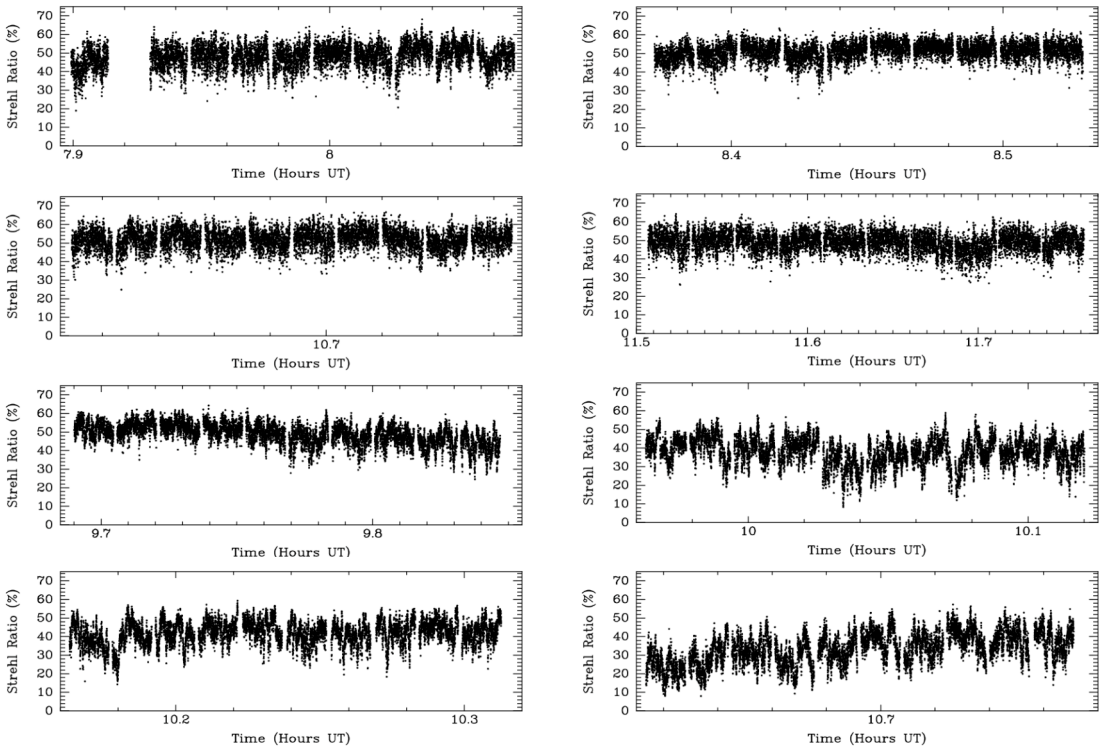

Fig. 1: Instantaneous Strehl ratio measurements from Lick Observatory.

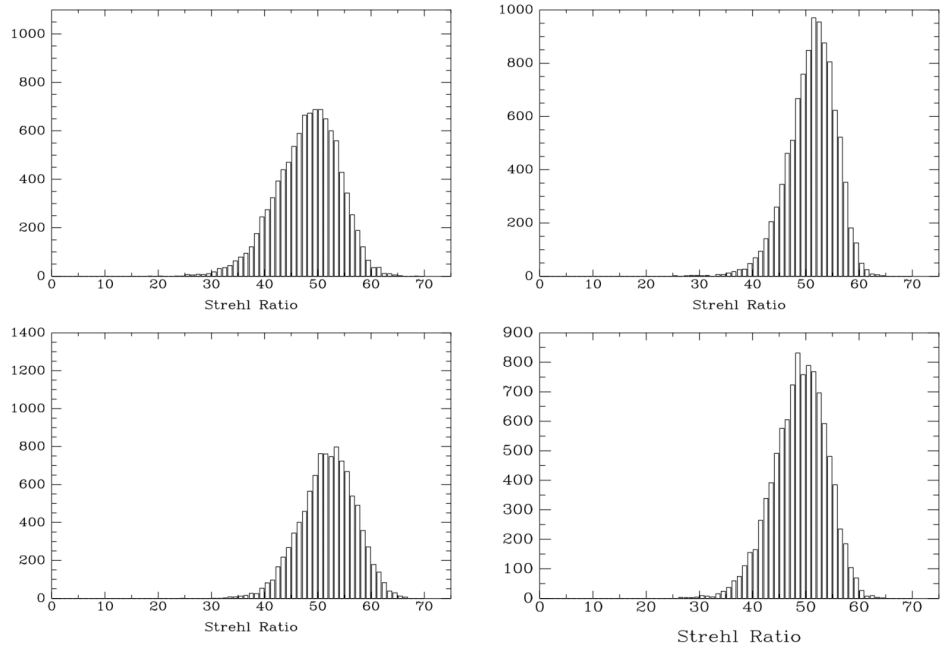

Fig. 2: Distribution of Strehl ratios for the top four plots in Figure 1. Note the similar non-Gaussian behavior with negative skewness.

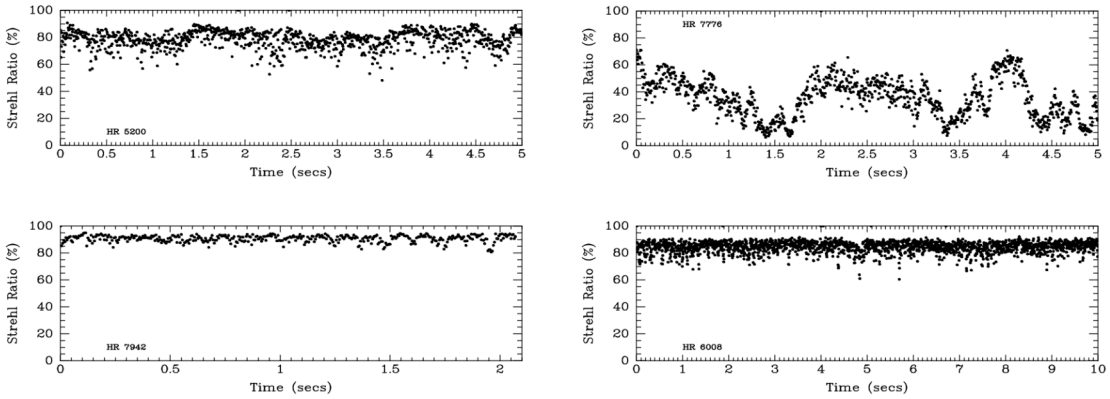

Fig. 3: Instantaneous Strehl ratio measurements from AEOS.

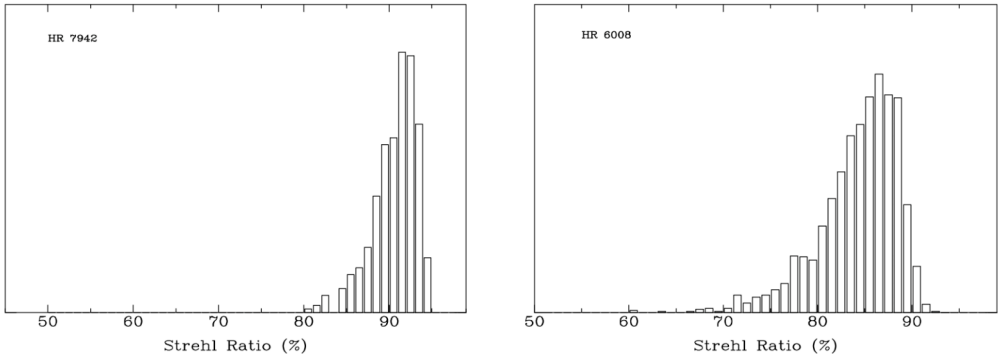

Fig. 4: Distribution of Strehl ratios for the bottom plots in Figure 3. Note the similar non-Gaussian behavior with negative skewness.

The Strehl ratio analysis of the AEOS data showed similar variability and distributions even though there is substantially less data (10 − 20%). Fig. 3 shows the instantaneous Strehl ratio variability for some of the AEOS data and illustrates that the compensation can be variable or stable. The high values of *S*, compared with previously reported focal plane AEOS Strehl ratio measurements, illustrate that other sources of aberration between the deformable mirror and the focal plane imaging are not taken into account. The ability to obtain simultaneous residual wavefront measurements along with focal plane PSF measurements will be very useful for analyzing the AO system's performance and locate the sources of further degradation of the wavefront between the two sensing planes. Fig. 4 shows the histograms for the bottom two quasi-stationary data sets shown in Fig. 3. These show similar negative skewness to the LO Strehl ratio histograms shown in Fig. 2.

3. THE MARECHAL APPROXIMATION

The AEOS data permits us to compare the measured Strehl ratios for the images to the phase variances for a working AO system. As mentioned earlier, the performance of an AO system is typically measured by the Strehl ratio metric *S* and this in turn is related back to the residual phase variance $\sigma_p^{\,2}$, the error of the AO system, by the Marechal approximation.

$$S \approx \exp\left(-\sigma_p^{\,2}\right)$$

Fig. 5 compares the rms of the residual phases as measured for the AEOS data to the Strehl ratios as measured directly from the numerically propagated Fourier plane images for seventeen different data sets comprising of 1000-2000 measurements per data set. The solid line is the Marachel approximation as given above. These data show a

very broad range of compensation with 10% < S < 95%. As can be seen, there is a very good agreement between the measurements and the prediction. However, there are a significant number of data points which are displaced from the line corresponding to larger phase variances for a given Strehl ratio. An investigation of the data explains the source of these deviations. The Strehl ratio is defined as the volume normalized intensity at the center of the image. In some of the AEOS data there is a residual tip-tilt error in the phases. The Strehl ratio values are obtained by actually measuring the image sub-pixel peak value as described in the previous section. If this peak value is not at the frame center then the phase variance will be higher because of a residual tilt term.

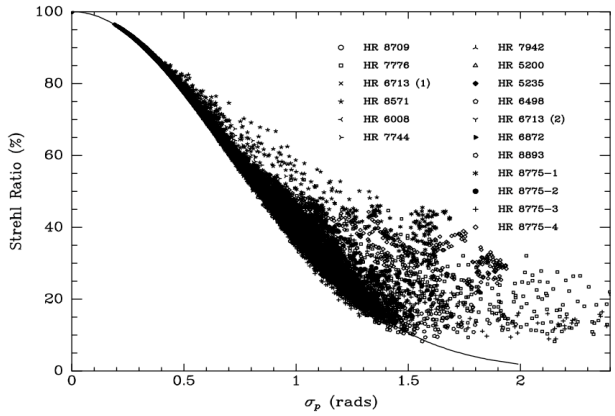

Fig. 5: The Marechal approximation (solid line) compared to the measurements of S and σ_p from the AEOS data.

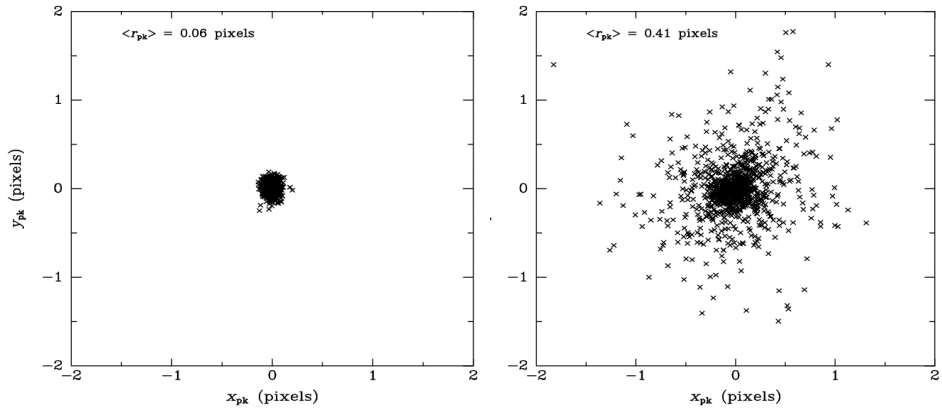

Fig. 6: Sub-pixel peak locations from the frame center for the AEOS measurements of HR 5200 (left) and HR 7776 (right).

Fig. 6 shows the (x,y) offset of the sub-pixel peak locations from the frame center for two of the AEOS data sets shown in Fig. 3. For the HR 5200 data, all data frames have a peak value very close to the center with a mean of 0.06 pixels whereas for the HR 7776 data there are a significant number of frames whose peak is much further away, with a mean of 0.41 pixels. The inclusion of those frames with relatively large peak offsets implies the presence of a residual tip-tilt term in the reconstructed phase maps. Fig. 7 shows the residuals between the predicted and the measured Strehl ratio measurements for those frames with a peak offset of ≤ 0.3 pixels. These plots illustrate that the predicted Strehl ratios underestimate the measured values as the latter decreases and also that the scatter increases. This is more clearly seen in the second panel which shows the mean and standard deviation within measured Strehl ratio bins of width S=10%. This illustrates the partial breakdown of the Marechal approximation for accurate determination of the Strehl ratio from the phase variance (and vice-versa) for S < 50%.

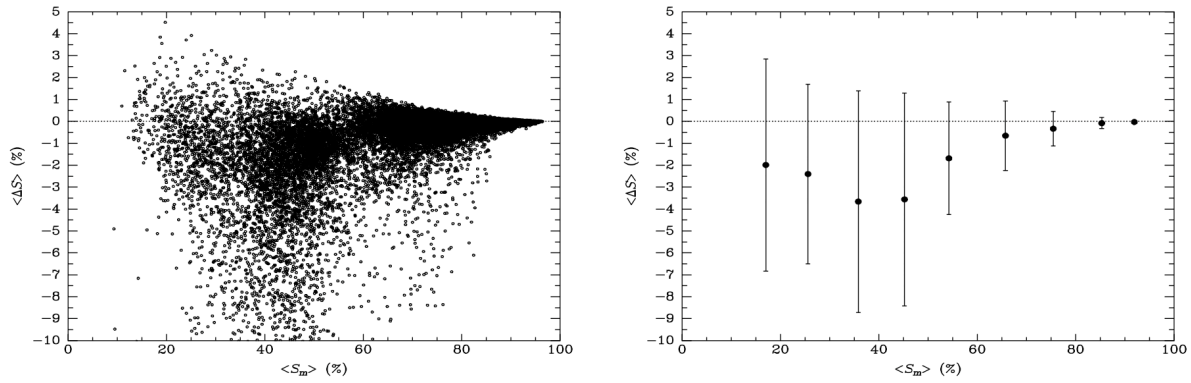

Fig. 7: Differences between Marechal-predicted and measured Strehl ratios for the individual frames (left) and in 10% bins.

4. DISTRIBUTION OF THE WAVEFRONT PHASE VARIANCE

The AEOS data gives us a unique opportunity to estimate the distribution of the phase variance. Fig. 8 shows the histograms of the phase variance for four quasi-stationary time series observed for four stars with AEOS. It is clear that the distribution possesses a positive skewness, i.e. an excess of high values is present.

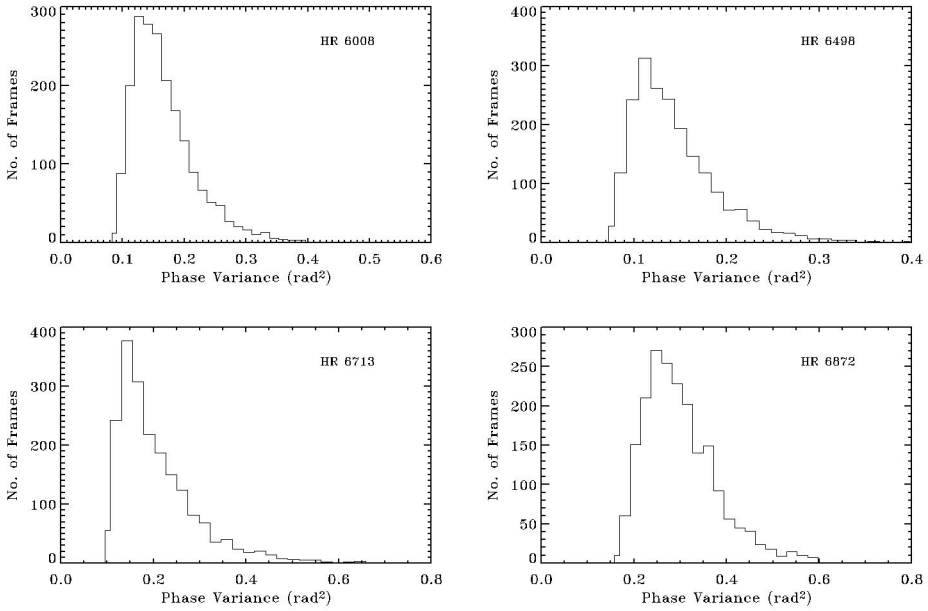

Fig. 8: Histograms of the phase variance for stars HR 6008, HR 6498, HR 6713 and HR 6872.

We hypothesize that the sample variance of the phase calculated from the actuator commands is distributed according to the gamma PDF. There are two assumptions in the following analysis: that the actuator commands come from a Gaussian distribution and that the commands are independent and identically distributed (i.i.d.). Phase perturbed by the atmosphere is a Gaussian random process by the Central Limit Theorem (CLT) [4]. The AO system can be thought of as high-pass spatial filter [5] acting on phase. In this last reference the simulated AO-corrected phase is obtained by inverse-transforming the product of the Fourier transform of atmospheric phase and the Fourier representation of the high-pass filter. This operation can be represented as a convolution in the spatial domain. The convolution integral can be written as a limit of approximating sums [6]. This means that AO-corrected phase at each spatial location can be thought of as a weighted sum of normally-distributed atmospheric phase values. The sum of any number of Gaussian random variables, dependent or independent, is itself Gaussian therefore the AO-

corrected phase is normally distributed. We can assume that actuator commands are also Gaussian since they estimate normal random variables – values of AO-corrected phase at actuator locations.

There is also another argument. The commands are obtained via multiplication of the control matrix, with dimensions equal to the number of actuators and twice the number of subapertures, and the centroids vector. In the case of AEOS system this means that every command is computed as a weighted sum of a great number, ~ 950, independent random variables (centroids). The possible dependence of centroids is not a problem as they are Gaussian random variables (see previous discussion of Gaussian AO-corrected phase). By the CLT, the resulting commands are normally distributed.

The aperture-averaged phase variance, σ^2, is estimated using the Maximum Likelihood (ML) estimator:

$$s^2 = \frac{1}{m}\sum_{i=1}^{m}\left(\hat{\phi}_i - \bar{\hat{\phi}}\right)^2$$

where $\hat{\phi}_i$, $i = 1,\ldots,m$, are the actuator commands (estimating true phase at a given location), $\bar{\hat{\phi}}$ is their mean. This ML sample variance follows a gamma distribution (Γ) if all $\hat{\phi}_i$ are independent and identically distributed [7]:

$$p\left(s^2\right) = \Gamma\left(\frac{m-1}{2}, \frac{2\sigma^2}{m}\right)$$

One can argue that the actuator commands should be identically distributed or spatially stationary if the Tip-Tilt (TT) module works perfectly. Otherwise, due to insufficient stroke, actuators would not be able to compensate for large excursions from the mean in some parts of the TT-corrected wavefront. Hence $\bar{\hat{\phi}}$ would be spatially dependent and the $\hat{\phi}_i$'s would not come from the same distribution. For a very high-order AO system like AEOS the residual phase deviations are driven very close to zero, so the assumption of spatial stationarity should be valid. Temporal stationarity will be rarely encountered due to significant temporal changes in atmospheric seeing, but those will be later removed with a de-trending procedure. It is also assumed that any spatial correlation between phase values at different locations in the wavefront, quantified by the coherence length r_0, is removed by the AO system. The last step is to remember that uncorrelated Gaussian random variables are also statistically independent (in pairs, within small wavefront patches).

The PDF of the gamma distribution is given by the formula:

$$p\left(x;k,\theta,\mu\right) = \frac{\left(\frac{x-\mu}{\theta}\right)^{k-1}\exp\left(-\frac{x-\mu}{\theta}\right)}{\Gamma\left(k\right)\theta} \quad \text{for } x \geq \mu$$

where $k > 0$ is the shape parameter, $\theta > 0$ is the scale parameter, and μ is the location parameter. The PDF is positively skewed, its mean is equal to $\mu + k\theta$ and variance is $k\theta^2$. Both exponential and χ^2 distributions are special cases of the gamma distribution.

The gamma distribution (for $\mu = 0$) has the property of constant coefficient of variation, defined as the ratio of the standard deviation to the expected value. For the two-parameter gamma distribution it's equal to $k^{-1/2}$. This means that during periods of poor seeing/poor compensation the phase sample variance will be more variable as the mean deviation scales linearly with the mean level of fluctuations. This effect was observed in the AEOS data (Fig. 9).

ARIMA (AutoRegressive Integrated Moving Average) modeling [8] was used to obtain i.i.d. random variables from the non-stationary phase variance data. It is a statistical method of discovering patterns in data and forecasting future values based on those patterns. It will be used here for the opposite goal – to obtain the values of i.i.d. "noise" and visually test its distribution. The result of the gamma PDF curve fitting for HR 6872 is shown in Fig. 10 which indicates that the gamma PDF provides a good fit to the phase variance distribution estimated from the actuator commands.

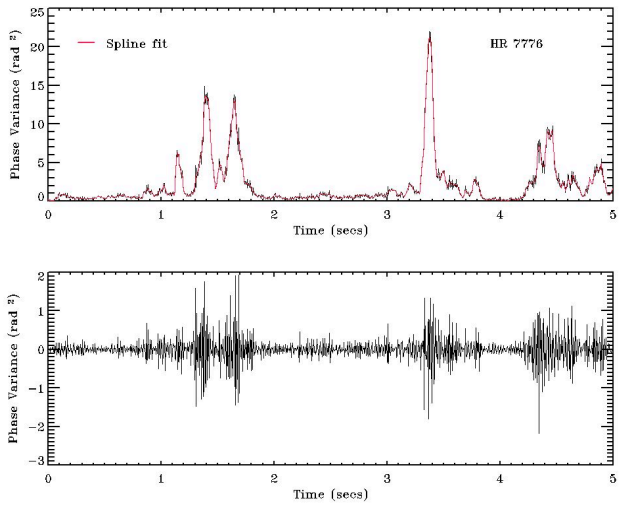

Fig. 9: Time series for the star HR 7776 (top) with the B-spline fit (no suitable ARIMA model could be found). Residuals are shown in the bottom panel.

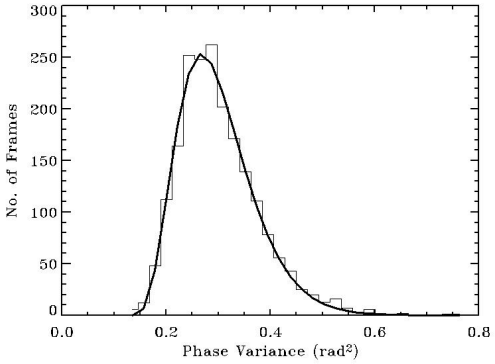

Fig. 10: Fit of the gamma distribution to the histogram of the phase variance for HR 6872. Residuals of the ARIMA model are centered on the series mean.

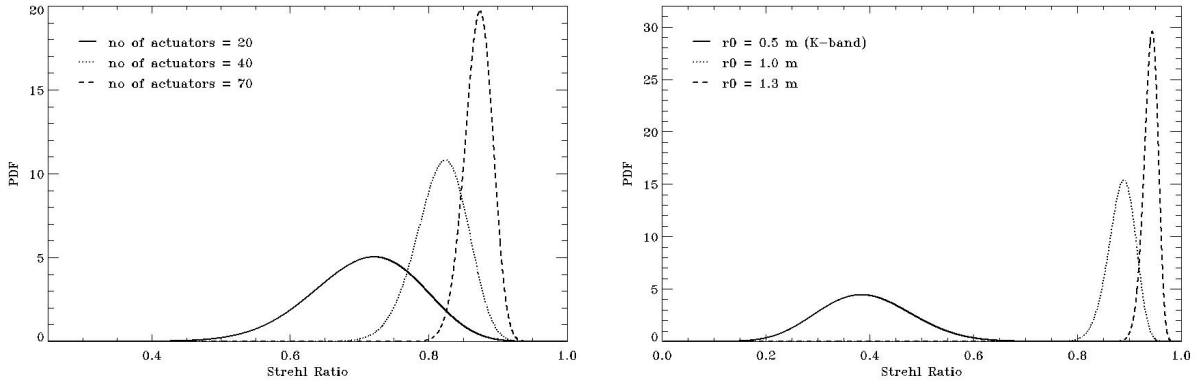

Fig. 11: (Left) Distributions of the Strehl ratio for three levels of actuator density, r_0 = 0.8m (*K*-band) and (Right) for three levels of turbulence strength when number of actuators is constant.

5. DISTRIBUTION OF THE INSTANTANEOUS STREHL RATIO

Given the distribution of the wavefront phase variance we can proceed to find the PDF of the instantaneous Strehl ratio using the earlier approach [2] linking the PDFs of instantaneous r_0 and instantaneous S. Marechal approximation is utilized again to arrive at the following result:

$$p_S(s) = \frac{p_{\text{var}}(-\ln s)}{s}$$

This means that, by substituting the opposite of the logarithm of the Strehl ratio into the phase variance PDF and dividing by that Strehl ratio, one obtains the value of PDF for that particular instance, s, of S. This simple result is a big improvement over the complex PDF(s) based on log-normal PDF(r_0) [2]. In this latter case the complicated dependence of s on r_0 meant that the resulting distribution function was also quite convoluted.

Now we can look at the distribution of the instantaneous Strehl ratio given m and σ^2. We will start by looking at what happens to PDF(s) when the level of correction (m) is increased. In the following sections it is assumed that the system utilizes a perfect tip-tilt correction, so that the Marechal approximation can be safely used (for $s > 0.1$). It has to be noted that the resulting plots are unrealistic, in the sense that the Strehl ratios are much higher than observed with real systems of similar complexity. This is to be expected, since other sources of error not mentioned here (e.g. non-common-path errors) result in lower real-life Strehl ratios.

Residual phase variance, σ^2, is decomposed into the fitting error, the bandwidth error and the error due to pure time delay [2]. Parameters of the Lick system were used in the latter two, while the fitting error depends on m – the number of actuators. Fig. 11 shows the resulting PDFs for m = 20, 40 and 70 as well as for different values of r_0 with a fixed number of actuators. For the former, the distributions are negatively skewed as expected and the variance of the PDF(s) decreases for higher m. For the latter, the variance of PDF(s) decreases for higher mean Strehl ratio (longer coherence lengths). Note that the skewness changes from positive to negative around s = 0.4. This effect could be verified if we had data from a poor-seeing night at Lick.

6. SUMMARY

We have investigated the instantaneous performance of two adaptive optics systems at Lick Observatory on Mt. Hamilton in California and at the Advanced Electro Optical System (AEOS) on Haleakala, Maui. For the former we used high speed focal plane data to estimate the instantaneous Strehl ratio S and for the latter we used the instantaneous phase variance maps from the wavefront sensor to numerically compute the point spread function for which the Strehl ratio was computed. Data from both systems showed similar distributions of the instantaneous Strehl ratio, asymmetric and negatively skewed. The AEOS data also showed the instantaneous residual phases of the wavefront to have a positively skewed asymmetric distribution. We have been able to model the residual phase distribution as a Γ-function and using this we have predicted the shapes of the observed Strehl ratio distributions. This analysis shows that the frame selection approach for image sharpening of speckle data [1,9] would not produce significantly sharper images when applied to AO-corrected data due to the lack of outliers (high Strehl ratio images).

The AEOS data has also permitted us to investigate the validity of the Marechal approximation for closed-loop AO data. We compared the predicted Strehl ratios from the Marachel approximation to those measured from the corresponding PSFs. We find that as the AO performance decreases the predicted Strehl ratios have a tendency to increasingly underestimate the measured by a few percent and that the scatter of these differences also increases.

ACKNOWLEDGEMENTS

This work has been supported by the National Science Foundation Science and Technology Center for Adaptive Optics, managed by the University of California at Santa Cruz under cooperative agreement No. AST–9876783 as well as COSMOGRID (Grid-enabled Computational Physics of Natural Phenomena). We would like to thank the staff of Lick Observatory, in particular Elinor Gates and Bryant Grigsby, the AO Support Scientists, for their valuable assistance with the AO system and with the data collection. In addition we'd like to thank Donald Gavel, Mike Fitzgerald, Remy Soummer, Nicholas Devaney and Granville Tunnicliffe-Wilson for very helpful and useful discussions.

REFERENCES

1. Baldwin, J. E., Tubbs, R. N., Cox, G. C., Mackay, C. D., Wilson, R. W., & Andersen, M. I., "Diffraction-limited 800nm imaging with the 2.56m Nordic Optical Telescope", *Astronomy and Astrophysics*, 368, L1-L4, 2001
2. Gladysz, S., Christou, J. C., & Redfern, M., "Characterization of the Lick adaptive optics point spread function", *Proceedings of SPIE*, 6272, 2006

3. Roberts, L. C., Jr., Perrin, M. D., Marchis, F., Sivaramakrishnan, A., Makidon, R. B., Christou, J. C., Macintosh, B. A., Poyneer, L. A., van Dam, M. A., & Troy, M., "Is that really your Strehl ratio?", *Proceedings of SPIE*, 5490, 504-515, 2004
4. Herman, B. J., & Strugala, L. A., "Method for inclusion of low-frequency contributions in numerical representation of atmospheric turbulence", *Proceedings of SPIE*, 1221, 183-192, 1990
5. Sivaramakrishnan, A., Koresko, C. D., Makidon, R. B., Berkefeld, T., & Kuchner, M. J., "Ground-based Coronagraphy with High-order Adaptive Optics", *Astrophysical Journal*, 552, 397-408, 2001
6. Goodman, J. W., *Statistical Optics*, New York: Wiley-Interscience, 2000
7. Kenney, J. F., & Keeping, E. S., *Mathematics of Statistics, Pt. 2*, Princeton, NJ: Van Nostrand, 1965
8. Box, G. E. P., & Jenkins, G. M., *Time series analysis: Forecasting and control*, San Francisco: Holden-Day, 1970
9. Redfern, R. M., Devaney, M. N., O'Kane, P., Ballesteros Ramirez, E., Gomez Renasco, R., & Rosa, F., "Image sharpening of time-tagged counts from a photon counting detector: application of a modified Wiener filter", *Mon. Not. R. Astron. Soc.*, 238, 791-806, 1989